

RESEARCH PAPER

Simulation of wheat growth and development based on organ-level photosynthesis and assimilate allocation

J. B. Evers^{1,*}, J. Vos¹, X. Yin¹, P. Romero², P. E. L. van der Putten¹ and P. C. Struik¹

¹ Centre for Crop Systems Analysis, Wageningen University, PO Box 430, 6700 AK Wageningen, the Netherlands

² Department of Viticulture, IMIDA, E-30150 la Alberca, Murcia, Spain

* To whom correspondence should be addressed: E-mail: jochem.evers@wur.nl

Received 23 October 2009; Revised 19 January 2010; Accepted 21 January 2010

Abstract

Intimate relationships exist between form and function of plants, determining many processes governing their growth and development. However, in most crop simulation models that have been created to simulate plant growth and, for example, predict biomass production, plant structure has been neglected. In this study, a detailed simulation model of growth and development of spring wheat (*Triticum aestivum*) is presented, which integrates degree of tillering and canopy architecture with organ-level light interception, photosynthesis, and dry-matter partitioning. An existing spatially explicit 3D architectural model of wheat development was extended with routines for organ-level microclimate, photosynthesis, assimilate distribution within the plant structure according to organ demands, and organ growth and development. Outgrowth of tiller buds was made dependent on the ratio between assimilate supply and demand of the plants. Organ-level photosynthesis, biomass production, and bud outgrowth were simulated satisfactorily. However, to improve crop simulation results more efforts are needed mechanistically to model other major plant physiological processes such as nitrogen uptake and distribution, tiller death, and leaf senescence. Nevertheless, the work presented here is a significant step forwards towards a mechanistic functional-structural plant model, which integrates plant architecture with key plant processes.

Key words: Assimilate allocation, crop model, functional-structural plant model, photosynthesis, shade avoidance, tillering, *Triticum aestivum*, wheat.

Introduction

Simulation models of crop growth and development are instrumental in predicting biomass accumulation and yield as driven by, for example, incoming solar radiation. In the case of wheat (*Triticum aestivum*), several of such process-based crop models have been developed in the past (Jamieson *et al.*, 1998; Van Ittersum *et al.*, 2003; Yin and Van Laar, 2005). In most of those modelling approaches, plants are not described individually; rather the area of leaves per unit soil surface area is simulated, which intercepts light based on exponential attenuation of radiation in relation to canopy depth (1D or the one-dimensional approach). Canopy photosynthesis rate is calculated using photosynthesis-light response curves or an even simpler radiation use efficiency approach is used. Several crop fractions are introduced representing, for example, the

leaves, roots, spikes, etc., which receive growth substrates according to fixed or dynamic assimilate partitioning fractions. For the purpose of yield prediction, this approach proves rather robust, albeit dependent on the choices made in the implementation of the model and on model calibration (Jamieson *et al.*, 1998).

However, the 1D approach can be too simple. There are many examples in which plant structure is a determinant factor, such as the impacts of leaf angle as influenced by genotype or water status, herbivory by insects, crop-weed competition, cutting and pruning, biocide spraying, and variation in plant population density. Systems in which such impacts are crucial are now increasingly being simulated using the concept of a functional-structural plant model (FSPM; Room *et al.*, 1996; Godin and Sinoquet, 2005;

Fourcaud *et al.*, 2008; Vos *et al.*, 2009). An FSPM is a plant model that explicitly takes into account plant structure in three dimensions (3D). Plant components such as leaves and stems and their geometrical properties like surface area, shape, and angle, are explicitly spatially represented in 3D.

In the recent past, members of the Poaceae family (grasses and cereals) have been rewarding subjects of research in the field of functional–structural plant modelling (Fournier *et al.*, 2007). Poaceae species usually exhibit a particularly regular and co-ordinated development making them particularly suitable for an FSPM. The models that have been reported up to now range from primarily descriptive (e.g. Buck-Sorlin, 2002; Evers *et al.*, 2005; Watanabe *et al.*, 2005; Dornbusch *et al.*, 2007) to (partially) mechanistic (e.g. Fournier and Andrieu, 1999; Guo *et al.*, 2006; Drouet and Pagès, 2007; Verdenal *et al.*, 2008). Our current study is based on an existing wheat model, ADELwheat (Fournier *et al.*, 2003; Evers *et al.*, 2005). This model is not an FSPM *sensu stricto*, since the model merely gives a detailed description of the three-dimensional development of wheat structure without taking into account the underlying mechanisms. Adding aspects of plant functioning would make the plant structure an emerging property of the model, rather than an input.

Therefore, the objective of this paper is to integrate the key aspects of plant functioning into the descriptive ADELwheat architectural model, by adding key processes of 3D-specific plant growth: (i) interception of photosynthetically active radiation by each individual phyto-element; (ii) assimilate acquisition based on a coupled biochemical photosynthesis–stomatal conductance model depending on organ-level intercepted radiation, temperature, and nitrogen content; and (iii) assimilate partitioning to those organs that require assimilates for growth. This results in an innovative model of wheat growth that simulates a feedback loop in which above-ground plant structure determines local light interception, which determines local photosynthesis and individual organ growth, which in turn determine above-ground plant structure. This upgraded model integrates key aspects of above-ground form and function of wheat plants, and simulates plant growth and development based on key exogenous and endogenous processes occurring at the level of the plant organ.

Materials and methods

Experiments

In order to parameterize the functional part of the model, two experiments were conducted. In experiment 1, spring wheat (cv. Minaret) plants were grown in a climate-controlled walk-in growth chamber of the phytotron of the Centre for Crop Systems Analysis of Wageningen University, at a population density of 508 plants m^{-2} . The soil per container had 3.47 g N, and was mixed with 28 g P_2O_5 and 8.4 g K_2O . N was added twice: 5.13 g before sowing and 2.16 g at stem elongation per container. The chamber lamps had an irradiance of 550–650 $\mu mol m^{-2} s^{-1}$ at canopy level. The photoperiod was 15 h d^{-1} , the relative humidity was 75%, and temperature was 16/11 °C (light/dark period) until the third leaf stage and 21/16 °C thereafter. Details on the experimental set-up

and the measurements can be found in Yin *et al.* (2009). Experiment 1 was used to gather data on (i) photosynthesis rates of individual wheat leaf blades allowing photosynthetic parameters for the model to be derived subsequently (see section ‘the wheat model’ below), and (ii) paired data of leaf nitrogen concentration and SPAD value (index for chlorophyll content, gathered in experiment 2) to determine a calibration curve estimating leaf N concentration from the SPAD reading.

Experiment 2 was performed outdoors under natural climatic conditions in Wageningen, the Netherlands (51° 58' N) from April to August 2006. Wheat plants were grown at three plant population densities: 100, 262, and 508 plants m^{-2} . The experimental set-up was similar to the ones in experiments described by Evers *et al.* (2006, 2007b). Experiment 2 was used to collect data on (i) leaf SPAD values (SPAD-502, Minolta Camera, Tokyo, Japan) to estimate leaf nitrogen concentration (g m^{-2}); (ii) plant organ length and mass to parameterize the sigmoid length–mass relationship of leaves (see section ‘plant organ development’ below) and the sink strength functions (see section ‘assimilate allocation’ below), and (iii) individual tiller appearance and leaf and tiller senescence.

The wheat model

The point of departure was an existing descriptive model of wheat architectural development called ADELwheat (Fournier *et al.*, 2003), which has been implemented using the plant modelling software cpfg (Mêch, 2004; Prusinkiewicz *et al.*, 2000), parameterized for spring wheat cv. Minaret and validated for several growing conditions (Evers *et al.*, 2005, 2007b). Figure 1 shows a visualized example of a small simulated wheat plot. To transform this descriptive wheat architectural model into a photosynthesis-based FSPM of spring wheat, functionality has been implemented at the level of the individual plant organ. This included the calculation of photosynthesis, respiration, and transpiration rates as influenced by local incident radiation, temperature, nitrogen content, vapour pressure deficit, and CO_2 concentration. Also, provisions were implemented for the calculation of assimilate distribution within the plant structure and for subsequent bud outgrowth and organ growth. The model was able to simulate development up until plant maturity.

Most of the concepts used here are well established and widely used. A significant part of the routines have been adapted from our GECROS crop model; see Yin and Van Laar (2005) and references therein. The equations related to photosynthesis, stomatal conductance, organ microclimate, and global environment, their relationships to leaf nitrogen content and temperature,



Fig. 1. Visualization of a virtual wheat canopy using the current model, illustrating the level of detail in plant structure that is considered in this modelling study.

and their variables and parameters have been described in the Supplementary data at *JXB* online (equations S1 to S39) as they have been published previously in various papers by our own group (Goudriaan and Van Laar, 1994; Yin *et al.*, 2004, 2009; Yin and Van Laar, 2005; Yin and Struik, 2009) and by other groups (Monteith, 1973; Farquhar *et al.*, 1980; Matthews and Hunt, 1994; de Pury and Farquhar, 1997; Bernacchi *et al.*, 2002). Equations related to radiation absorption, assimilate allocation, and plant organ development are outlined below. All variables and parameters described in this paper (including those used in the Supplementary data available at *JXB* online) are listed in Table 1, with their units.

Absorbed radiation

Variables I_{inc} (equation S16) and I_{abs} (equation S28) were calculated for individual leaves using the Nested Radiosity light model (NR) (Chelle and Andrieu, 1998), in combination with a mathematical description of the global incoming radiation I (equation S35). NR calculated the light absorbed by each individual plant organ, for any wavelength or set of wavelengths. In the current wheat model a plant organ such as a leaf was defined by a set of polygons, the vertices of which determine their positions in space. Absorption, reflection, and transmission of light at the level of a module, for example, a leaf blade, were calculated by summing the contributions of the polygons that comprise the module. This was done internally in NR, i.e. the output of NR was at the whole-leaf level.

In the current implementation, the source of the incoming light was a virtual hemisphere, approximated by 36 point sources (see Fig. 1 in Evers *et al.*, 2007a). A global incoming radiation of 1 (arbitrary rate unit) was assumed in NR, and NR subsequently estimated relative absorbed radiation by a leaf (I_{NR}) taking into account the optical properties of all neighbouring leaves (transmittance f_t and reflectance f_r , obtained from measurements on leaves of separately grown wheat plants using an Ocean Optics SD2000 spectrometer (Ocean Optics, Dunedin, Florida, USA). This resulted in a value of I_{NR} between 0 and 1 for each leaf. I_{abs} was then calculated by:

$$I_{\text{abs}} = I \times I_{\text{NR}} \quad (1)$$

where I is incoming radiation (W m^{-2} ; see equation S35 at *JXB* online). The combination of this calculated incoming radiation and the simple virtual hemisphere as described above, basically mimicked diffuse light (i.e. light coming from all directions) at an intensity comparable to normal daylight at the latitude of the Netherlands. Atmospheric transmissivity (τ), which was used in the calculation of I (see equation S35 at *JXB* online) and of leaf net absorbed radiation (see equations S28 and S29 at *JXB* online), was calibrated such as to ensure correspondence between simulated and observed daily radiation for the duration of experiment 2. In addition, calculations were made with a more realistic sky; see section ‘model sensitivity’ below.

Variable I_{abs} was used to calculate leaf temperature (see equation S28 at *JXB* online). To calculate electron transport rate (see equation S16 at *JXB* online), only the PAR fraction of I_{abs} was considered, and the value was converted from W m^{-2} into $\mu\text{mol m}^{-2} \text{s}^{-1}$ [factors of 0.55 and 4.55, respectively; both from Goudriaan and Van Laar (1994)]. Furthermore, the value was corrected for the light absorption of the leaf, since calculation of electron transport requires incident rather than absorbed radiation (see equation S16 at *JXB* online):

$$I_{\text{inc}} = \frac{I_{\text{abs}} \times 0.55 \times 4.55}{1 - f_r - f_t} \quad (2)$$

For leaf sheaths and internodes, procedures regarding organ microclimate were identical with one exception. Sheaths and internodes, represented in the model by a stem segment (cylinder) were defined as opaque objects, i.e. objects not transmitting any light.

Assimilate allocation

The net photosynthesis rate A per unit leaf area ($\mu\text{mol m}^{-2} \text{s}^{-1}$; see equation S1 at *JXB* online) was converted into an hourly rate per leaf (A_h in $\mu\text{mol leaf}^{-1} \text{h}^{-1}$) by:

$$A_h = A \times 3600 \times w \quad (3)$$

where w is the surface area of the leaf (m^2 , derived from plant architecture). Hourly mitochondrial respiration rate of a leaf ($R_{\text{d,h}}$) was calculated identically. Using A_h and $R_{\text{d,h}}$, daily gross assimilated CO_2 per leaf (A_1 in $\mu\text{mol leaf}^{-1} \text{d}^{-1}$) was calculated by adding the hourly rates of net photosynthesis rate and mitochondrial respiration of one day, based on the calculated day length (see equation S39 at *JXB* online). The values of A_1 of all leaves were summed to arrive at the daily gross assimilated CO_2 by the whole plant (A_G in $\mu\text{mol plant}^{-1} \text{d}^{-1}$). Subsequently, the daily net substrate available for growth (B_N) was estimated using the following equation:

$$B_N = (m_{\text{CO}_2} \times A_G \times 10^{-3} - r_m \times m_{\text{plant}}) \times f_{\text{CO}_2} + B_P \quad (4)$$

where m_{CO_2} is CO_2 molar mass (g mol^{-1}), and r_m is the fraction of total plant mass (m_{plant} in mg) that is subtracted from the amount of available substrates and used by the plant for maintenance respiration per day ($0.016 \text{ g CO}_2 \text{ g}^{-1} \text{ plant mass d}^{-1}$ at 20°C , using a Q_{10} value of 2 to calculate the effect of temperature on r_m ; Penning de Vries *et al.*, 1989). Multiplying by 10^{-3} converts μg to mg. Variable B_P is the pool of substrates (stored as sugars) that is available for growth (mg), and f_{CO_2} is a conversion factor from grams of CO_2 to grams of wheat biomass, of which the value (0.6067) was derived following equation 5:

$$f_{\text{CO}_2} = \frac{12/44}{0.45} \quad (5)$$

where 12/44 is the carbon mass fraction in CO_2 and 0.45 is the carbon mass fraction in wheat biomass (Vos, 1981).

The available substrate (B_N) was distributed among all growing organs (leaves, internodes, panicles, roots) using the relative sink strength principle (Heuvelink, 1996):

$$D_{r,i} = \frac{D_i}{\sum_{i=1}^n D_i} \quad (6)$$

where $D_{r,i}$ is relative sink strength of an organ i (dimensionless), D_i is its absolute sink strength (expressed as potential growth rate in mg substrate $\text{organ}^{-1} \text{d}^{-1}$), and n is the total number of sink organs. An important assumption of the relative sink strength principle is that all assimilates anywhere in the plant are equally available to all competing sinks.

D_i is calculated according to a bell-shaped curve based on the first derivative of the beta growth function, a flexible sigmoid three-parameter function that can represent various (asymmetric) sigmoid patterns (Yin *et al.*, 2003). Here, the beta growth function was simplified using the assumption that the time of maximum growth rate equals half the final elongation duration of an organ ($t_m = 0.5t_e$):

$$D_i = \begin{cases} \frac{D_c}{1-r_g} \cdot \frac{t(t_e-t)}{0.25 \cdot t_e^2} & t < t_e \\ 0 & t \geq t_e \end{cases} \quad (7)$$

where t_e is the final elongation duration of an organ ($^\circ\text{Cd}$), t is the amount of thermal time that has passed since the start of organ elongation ($^\circ\text{Cd}$), r_g is the fraction of potential substrate lost to growth respiration, and D_c is the maximum sink strength, defined as (Yin *et al.*, 2003):

$$D_c = \frac{1.5 \times W_{\text{max}}}{t_e} \quad (8)$$

Table 1. List of model variables and parameters, their definitions, and their units

Variable/parameter	Definition	Unit
A	Net photosynthesis rate	$\mu\text{mol CO}_2 \text{ m}^{-2} \text{ leaf s}^{-1}$
a_1	Empirical parameter in the f_{vpd} equation	–
A_G	Gross assimilated CO_2 by the plant	$\mu\text{mol plant}^{-1} \text{ d}^{-1}$
A_h	Net photosynthesis rate per leaf	$\mu\text{mol leaf}^{-1} \text{ h}^{-1}$
a_l	Parameter related to season-dependent solar shift	–
A_l	Gross assimilated CO_2 per leaf	$\mu\text{mol leaf}^{-1} \text{ d}^{-1}$
a_k	Slope parameter in the linear relationship between $\kappa_{2(\text{LL})}$ and N_l	$\text{mol e}^- \text{ m}^{-2} \text{ leaf mol}^{-1} \text{ photons g}^{-1} \text{ N}$
b_1	Empirical parameter in the f_{vpd} equation	kPa^{-1}
b_l	Parameter related to season-dependent solar amplitude	–
B_N	Net substrate available for growth	$\text{mg plant}^{-1} \text{ d}^{-1}$
B_P	Pool of substrates	mg plant^{-1}
b_k	Intercept parameter in the linear relationship between $\kappa_{2(\text{LL})}$ and N_l	$\text{mol e}^- \text{ mol}^{-1} \text{ photons}$
C	CO_2 concentration of the air	$\mu\text{mol mol}^{-1}$
c_a	CO_2 partial pressure of the air	μbar
c_c	CO_2 chloroplast partial pressure	μbar
c_i	Intercellular CO_2 partial pressure	μbar
C_i^*	Intercellular CO_2 compensation point	μbar
cpn	Cumulative phytomer number	phytomers
d	Day of the year	d
D_c	Maximum sink strength	$\text{mg substrate organ}^{-1} \text{ d}^{-1}$
$D_{f,i}$	Relative sink strength of an organ i	–
D_i	Absolute sink strength of an organ i	$\text{mg substrate organ}^{-1} \text{ d}^{-1}$
$D_{J_{\text{max}}}$	Deactivation energy of J_{max}	J mol^{-1}
E_p	Potential leaf transpiration	mm s^{-1}
$e_{S(\text{Ta})}$	Saturated vapour pressure of the air	kPa
$e_{S(\text{Tl})}$	Saturated vapour pressure at the leaf	kPa
E_X	Activation energy for parameter X (with X being either J_{max} , R_d , $V_{O/C}$, $V_{c,\text{max}}$, K_{mC} or K_{mO})	J mol^{-1}
f_{clear}	Fraction of net absorbed radiation accounting for sky clearness	–
f_{CO_2}	Conversion factor from grams of CO_2 to grams of wheat biomass	–
f_r	Leaf radiation reflectance	–
f_t	Leaf radiation transmittance	–
f_{vap}	Fraction of net absorbed radiation accounting for vapour pressure	–
f_{vpd}	Lumped parameter representing the VPD effect on stomatal conductance	–
g_0	Residual stomatal conductance for CO_2 at the light compensation point	$\text{mol m}^{-2} \text{ leaf s}^{-1} \text{ bar}^{-1}$
g_m	Mesophyll conductance for CO_2 diffusion	$\text{mol m}^{-2} \text{ leaf s}^{-1} \text{ bar}^{-1}$
g_s	Stomatal conductance for CO_2 diffusion	$\text{mol m}^{-2} \text{ leaf s}^{-1} \text{ bar}^{-1}$
h	Hour of the day in the sun height equation	h
H	Crop height	m
h_{dawn}	Hour of sunrise	h
h_{dusk}	Hour of sunset	h
i	Hour of the day in the air temperature equation	h
I	Incoming radiation	$\text{W m}^{-2} \text{ ground}$
I_{abs}	Amount of absorbed radiation	$\text{W m}^{-2} \text{ leaf}$
I_{inc}	Amount of PAR intercepted	$\mu\text{mol photons m}^{-2} \text{ leaf s}^{-1}$
I_{NR}	Relative absorbed radiation	–
J	Rate of electron transport	$\mu\text{mol e}^- \text{ m}^{-2} \text{ leaf s}^{-1}$
J_{max}	Maximum electron transport rate at saturating light levels	$\mu\text{mol e}^- \text{ m}^{-2} \text{ leaf s}^{-1}$
$j_{S/D}$	Supply/demand ratio threshold for bud outgrowth	–
K_{mC}	Michaelis-Menten constants for CO_2	μbar
K_{mO}	Michaelis-Menten constants for O_2	mbar
k_N	Slope parameter in the N_l equation	–
lat	Latitude	°
m_{CO_2}	CO_2 molar mass	g mol^{-1}
m_{plant}	Total plant mass	mg
N_l	Total organic leaf nitrogen	$\text{g N m}^{-2} \text{ leaf}$
$N_{l,b}$	Minimum amount of leaf nitrogen below which photosynthesis rate is zero	$\text{g N m}^{-2} \text{ leaf}$
O	Oxygen partial pressure of the air	mbar
p_a	Slope parameter in the SPAD equation	$^{\circ}\text{Cd}^{-3} \text{ phytomer}^{-1}$

Table 1. Continued

Variable/parameter	Definition	Unit
p_b	Intercept parameter in the SPAD equation	$^{\circ}\text{Cd}^{-3}$
q_a	Slope parameter in the SPAD equation	$^{\circ}\text{Cd}^{-2} \text{ phytomer}^{-1}$
q_b	Intercept parameter in the SPAD equation	$^{\circ}\text{Cd}^{-2}$
R	Universal gas constant	$\text{J K}^{-1} \text{ mol}^{-1}$
r_a	Slope parameter in the SPAD equation	$^{\circ}\text{Cd}^{-1} \text{ phytomer}^{-1}$
r_b	Intercept parameter in the SPAD equation	$^{\circ}\text{Cd}^{-1}$
r_{bh}	Boundary layer resistance to heat	s m^{-1}
r_{bw}	Boundary layer resistance for water	s m^{-1}
R_d	Mitochondrial respiration rate	$\mu\text{mol CO}_2 \text{ m}^{-2} \text{ leaf s}^{-1}$
$R_{d,h}$	Net respiration rate per leaf	$\mu\text{mol h}^{-1}$
r_g	Fraction of potential substrate lost to growth respiration	–
RH	Relative humidity of the air	–
r_m	Fraction of total plant mass used for maintenance respiration	$\text{g mass g}^{-1} \text{ CO}_2$
R_n	Net absorbed radiation	$\text{J m}^{-2} \text{ s}^{-1}$
$r_{sw,p}$	Stomatal resistance to water transfer	s m^{-1}
r_t	Turbulence resistance to heat	s m^{-1}
r_{tb}	Combined turbulence and boundary layer resistance for CO_2	$\text{m}^2 \text{ leaf s bar}^{-1} \text{ mol}^{-1}$
s	Slope in the relationship of saturation vapour pressure to temperature	kPa K^{-1}
s_a	Slope parameter in the SPAD equation	phytomer^{-1}
s_b	Intercept parameter in the SPAD equation	–
SC	Solar constant	$\text{W m}^{-2} \text{ ground}$
$S_{c/O}$	Relative CO_2/O_2 specificity factor for Rubisco	$\text{mbar } \mu\text{bar}^{-1}$
S_j	Entropy term in the equation for J_{\max}	$\text{J K}^{-1} \text{ mol}^{-1}$
t	Amount of thermal time that have passed since The start of organ elongation	$^{\circ}\text{Cd}$
T_a	Temperature of the air	$^{\circ}\text{C}$
t_e	Final elongation duration of an organ	$^{\circ}\text{Cd}$
$tilt$	Tilt of the earth axis	$^{\circ}$
T_l	Leaf temperature	$^{\circ}\text{C}$
T_{\max}	Maximum daily air temperature	$^{\circ}\text{C}$
T_{\min}	Minimum daily air temperature	$^{\circ}\text{C}$
tt	Thermal time since plant emergence	$^{\circ}\text{Cd}$
u	Wind speed	m s^{-1}
V	Vapour pressure of the air	kPa
$V_{c,\max}$	Maximum carboxylation rate	$\mu\text{mol CO}_2 \text{ m}^{-2} \text{ s}^{-1}$
$V_{O/C}$	Ratio of maximum oxygenation to carboxylation rate of Rubisco	–
VPD_a	Vapour pressure deficit of the air	kPa
VPD_l	Leaf-to-air vapour pressure difference	kPa
w	Leaf surface area	m^2
w_l	Leaf blade width	m
W_{\max}	Maximum final organ biomass	mg organ^{-1}
Z	SPAD value	–
β	Height of the sun	$^{\circ}$
γ	Psychrometric constant	kPa K^{-1}
Γ^*	CO_2 compensation point	μbar
δ	Declination of the sun	$^{\circ}$
θ	Convexity factor for the electron transport rate equation	–
$K_{2(LL)}$	Conversion efficiency of incident PAR into electron transport at limiting light levels	$\text{mol e}^{-} \text{ mol}^{-1} \text{ photons}$
λ	Latent heat of vaporization of water	$\text{J kg}^{-1} \text{ water}$
ρ_{cp}	Volumetric heat capacity of air	$\text{J m}^{-3} \text{ K}^{-1}$
σ	Stefan–Boltzmann constant	$\text{J m}^{-2} \text{ s}^{-1} \text{ K}^{-4}$
τ	Atmospheric transmissivity	–
χ_J	Slope parameter in the linear relationship between $J_{\max 25}$ and N_l	$\mu\text{mol e}^{-} \text{ g}^{-1} \text{ N s}^{-1}$
χ_V	Slope parameter in the linear relationship between $V_{c,\max 25}$ and N_l	$\mu\text{mol CO}_2 \text{ g}^{-1} \text{ N s}^{-1}$

where W_{\max} is maximum final biomass (mg organ^{-1}) for leaves, internodes, panicles, and roots. Values for parameter W_{\max} of the various organ types were taken from experiment 2; t_e values were

taken from the original ADELwheat parameterization (Fournier *et al.*, 2003). To estimate the daily amount of substrate that was allocated to a sink organ (B_i), the following equation was used:

$$B_i = \min(D_{f,i} \times B_N, D_i) \quad (9)$$

If $D_{f,i} \times B_N$ (representing substrate available to the organ) is higher than sink strength D_i , the difference was added to a plant-wide substrate pool (B_P) which was added to B_N the next day (as shown in equation 4). B_i was added daily to organ biomass m_i after subtracting potential substrate lost to growth respiration ($r_g \times B_i$). The substrate pool (B_P) and m_i values of all organs were added daily to arrive at total plant mass (m_{plant}), used in equation 4.

Plant organ development

Dimensions of leaves were calculated using an empirical sigmoid relationship between leaf mass and leaf length, derived from experiment 2. The supply/demand ratio (S/D) of the plant each day was used to determine outgrowth of buds into tillers. The value of S/D was calculated as:

$$S/D = B_N / \sum_{i=1}^n D_i \quad (10)$$

S/D is dimensionless, since both nominator and denominator are expressed in units of mg substrate $\text{plant}^{-1} \text{d}^{-1}$. After having been initiated (i.e. after a new phytomer has been formed by the apex), buds were allowed to grow out only if S/D was larger than a threshold value $j_{S/D}$. This check was performed daily. Therefore, if bud outgrowth was suppressed on one day, outgrowth could still occur the next day, if S/D was higher than $j_{S/D}$ that day. The ability of a bud to grow out was removed when the internode of the preceding phytomer started to extend; this is in accordance with personal observations and literature (Williams and Langer, 1975). Buds that remained at soil level (i.e. that did not have an extending internode below it) maintained the possibility to grow out in favourable conditions. This allows for tiller regrowth, a phenomenon that can be observed in wheat, for example, when mature stems lodge. Tiller and leaf senescence were not modelled mechanistically but implemented using input tables (for time of senescence and in the case of tillers also for the probability of senescence), based on empirical data from experiment 2. Remobilization of carbon was not taken into account at this stage.

Simulations

Each simulation comprised calculation of growth and development of 16 wheat plants, arranged in a 4×4 grid, resulting in $n=16$ per data point. There was no simulation of neighbouring plants outside this grid, so the simulated plot was exposed to light at all of its edges. Simulations were done using plant population densities similar to those used in the outdoor experiment (100, 262, and 508 plants m^{-2} ground). Seed orientation was chosen randomly. Starting day of the simulations was 1 April. The time steps of the model were 1 h for the calculation of photosynthesis, and 1 d for the calculation of assimilate allocation and updating of plant structure. For computational reasons, calculation of light distribution in the 3D canopy was done using a daily time step instead of an hourly time step (see section 'absorbed radiation' above), assuming plant structure does not significantly change from hour to hour, but only from day to day.

To evaluate model performance in terms of canopy photosynthesis rates and biomass accumulation and distribution, parameter $j_{S/D}$ was set to a default value of 0.500 in the first instance. Subsequently, values for $j_{S/D}$ of 0.250 and 0.375 were used as well to analyse the effect on bud outgrowth and subsequent tiller production. In the results section model output is shown mainly as m^{-2} of ground area [canopy gross assimilation rate, canopy sink strength, canopy shoot mass (increment)], based on plant population densities of the experimental plots. Exceptions are net photosynthesis rate, potentially allocatable substrate and sink strength (organ level) and number of living tillers (plant level).

Sensitivity analysis

In order to assess model output in response to changes in input parameters, a sensitivity analysis was performed on several key model parameters which were expected to have a significant influence on model output: atmospheric transmissivity (τ) which heavily depends on degree of cloudiness of the sky; growth and maintenance respiration (r_g and r_m); and maximum organ biomass (W_{max}). These parameters were decreased and increased by 10% and 20% of their default values, and variation in output was recorded for two output variables: final above-ground canopy biomass and maximum number of tillers produced per plant. If possible, the degree of sensitivity to input modulation was expressed as a linear regression of the relative change in output on the relative change in input; this served to check for systematics in the effect of variable change. The slope of the regression line (the elasticity), represented the relative change in model output per amount of the relative change in the value of the input parameter. If the relative effect was larger than the relative change (i.e. if elasticity was larger than 1), a small change in the input variable had a disproportionate effect, which means that the calibration of the variable in question has to be done very accurately. Sensitivity analysis was done using a plant population density of 262 plants m^{-2} and a $j_{S/D}$ value of 0.5.

Also the sensitivity to the complexity of the virtual sky was investigated. Standard simulations used a virtual hemisphere as described above. Additional simulations were performed using a more realistic hemisphere (M Chelle, personal communication) representing the situation at $51^\circ 58' \text{N}$ at 1 May (Fig. 2a, b, c). This virtual hemisphere contained (i) light sources which together represent diffuse light (open bubbles), of which the relative light intensity depended on their location in the sky, and (ii) direct light sources representing the course of the sun (filled bubbles).

Results

Assimilation and allocation of assimilates

Photosynthesis rates ranged from approximately -0.5 to $20 \mu\text{mol CO}_2 \text{m}^{-2} \text{s}^{-1}$ (Fig. 3). Every spike in the diagrams represents one day (the top of the spike occurring around solar noon). The progressive widening of the daily photosynthesis spikes caused by the increasing air temperature as the season progressed, is obvious. Generally, a slight decrease in photosynthesis rate during the lifetime of most leaves could be observed, caused by increased shading by neighbouring leaves as well as by declining nitrogen content (and the associated photosynthetic capacity) of the leaves themselves. In agreement with general observations on grasses and cereals, Fig. 3 indicates that, commonly, four leaves were active at any time, except after the cessation of leaf appearance when the crop senesced. Maximum canopy gross assimilation rate was *c.* 125, 175, and $240 \text{g CO}_2 \text{m}^{-2} \text{ground area d}^{-1}$ for 100, 262, and 508 plants m^{-2} , respectively (Fig. 4). For 100, 262, and 508 plants m^{-2} , canopy sink strength reached peak values of *c.* 60, 75, and $115 \text{g m}^{-2} \text{d}^{-1}$, respectively (Fig. 5). Maximum values were *c.* 53, 78, and $105 \text{g m}^{-2} \text{d}^{-1}$, for 100, 262, and 508 plants m^{-2} , respectively (Fig. 6), reaching shoot mass values of *c.* 1500, 2200, and 2900g m^{-2} , respectively (inset in Fig. 6).

An example of how the assimilates were allocated to individual organs is shown in Fig. 7. Allocated substrate

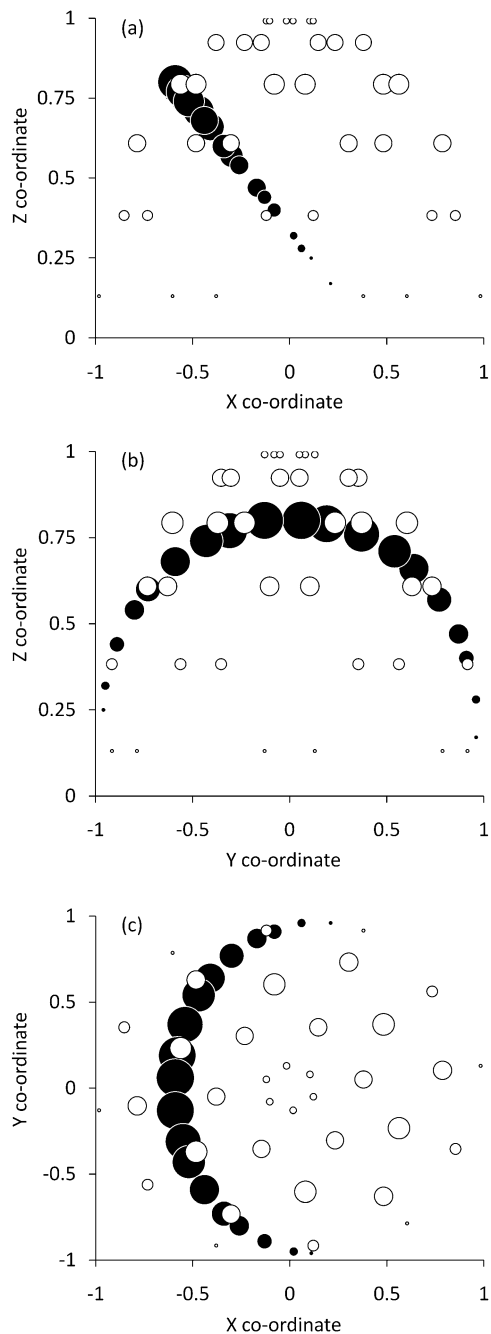


Fig. 2. (a, b, c) Configuration of the light sources of the virtual hemisphere, as used in the sensitivity analysis for sky complexity, viewed from two sides (a, b) and from the top (c). The axes represent the X, Y, and Z co-ordinates of the light sources; the size of the bubbles indicates the relative intensity of the light source it represents. The filled bubbles represent direct light (solar trajectory), the open bubbles comprise diffuse light coming from all directions.

(i.e. growth) of the organs was always the smaller of either potentially allocatable substrate or sink strength (see equation 9). Figure 7 depicts both sink strength and potentially allocatable substrate (according to equation 6) for internodes 5–9 of the main stem. In the case of

internodes 5–8, substrate potentially allocatable to an organ was lower than the sink strength of that organ. An exception can be observed in the case of internode 9.

Final values of two output variables were calculated. Harvest index, the proportion of grain mass in final shoot mass, decreased with increasing plant population density (values were 0.41, 0.43, and 0.49 for 100, 262, and 508 plants m^{-2}). Final radiation use efficiency, which expresses the amount of biomass formed MJ^{-1} of PAR absorbed, decreased with increasing population density: values were 1.99 (100 plants m^{-2}), 1.84 (262 plants m^{-2}), and 1.77 $g MJ^{-1}$ (508 plants m^{-2}).

Outgrowth of buds into living tillers was affected by plant population density and the value of $j_{S/D}$ as shown in Fig. 8a, b, and c. At 100 plants m^{-2} (Fig. 8a), the effect of alternative values of $j_{S/D}$ in the simulations resulted in differences in the moment at which the number of tillers increased to its maximum value, rather than in the maximum number of tillers. A $j_{S/D}$ value of 0.250 was closest to the experimental data. Across all $j_{S/D}$ values, tiller number was lower at 262 than at 100 plants m^{-2} . At 508 plants m^{-2} (Fig. 8c), qualitatively the simulated output in terms of tiller numbers was comparable to that at 262 plants m^{-2} . The moment of appearance of individual tillers was affected by the value of $j_{S/D}$ (Fig. 9): an increase in $j_{S/D}$ resulted in delayed tiller appearance. This trend was noticeable for all tillers but t1 and t2 (i.e. first order tillers no. 1 and 2, respectively), due to the seed reserves not having been depleted at the time of bud outgrowth. In addition to delay of appearance, a reduction in frequency of appearance due to increase in $j_{S/D}$ could also be observed in the simulation output.

Model sensitivity

The simulated final canopy biomass responded to changing the value of the maximum organ biomass parameter (W_{max}) with an elasticity of 0.74 ($R^2=0.82$): every per cent change in the value of W_{max} caused a change in final biomass of 0.74% on average, in the same direction. In terms of maximum number of tillers produced per plant, elasticity was highly sensitive at -2.5 ($R^2=0.94$). Modulating atmospheric transmissivity (τ) resulted in an elasticity value of -1.2 ($R^2=0.85$) for maximum tiller number; final biomass showed a non-systematic irregular response to variation in τ , therefore elasticity could not be calculated reliably. Variation in growth respiration (r_g) resulted in elasticity values of -0.41 ($R^2=0.69$) for final biomass and -1.8 ($R^2=0.72$) for maximum tiller number. Variation in maintenance respiration (r_m) on either final biomass or maximum tiller number was not systematic.

Using the more complex, realistic virtual sky yielded remarkable results. Using default simulation settings (population density of 262 plants m^{-2} , and a $j_{S/D}$ value of 0.500), the more realistic sky resulted in a considerable increase in light interception compared with using the standard sky (an increase of 39.9% on average). However, canopy gross assimilation rate and canopy biomass were only slightly

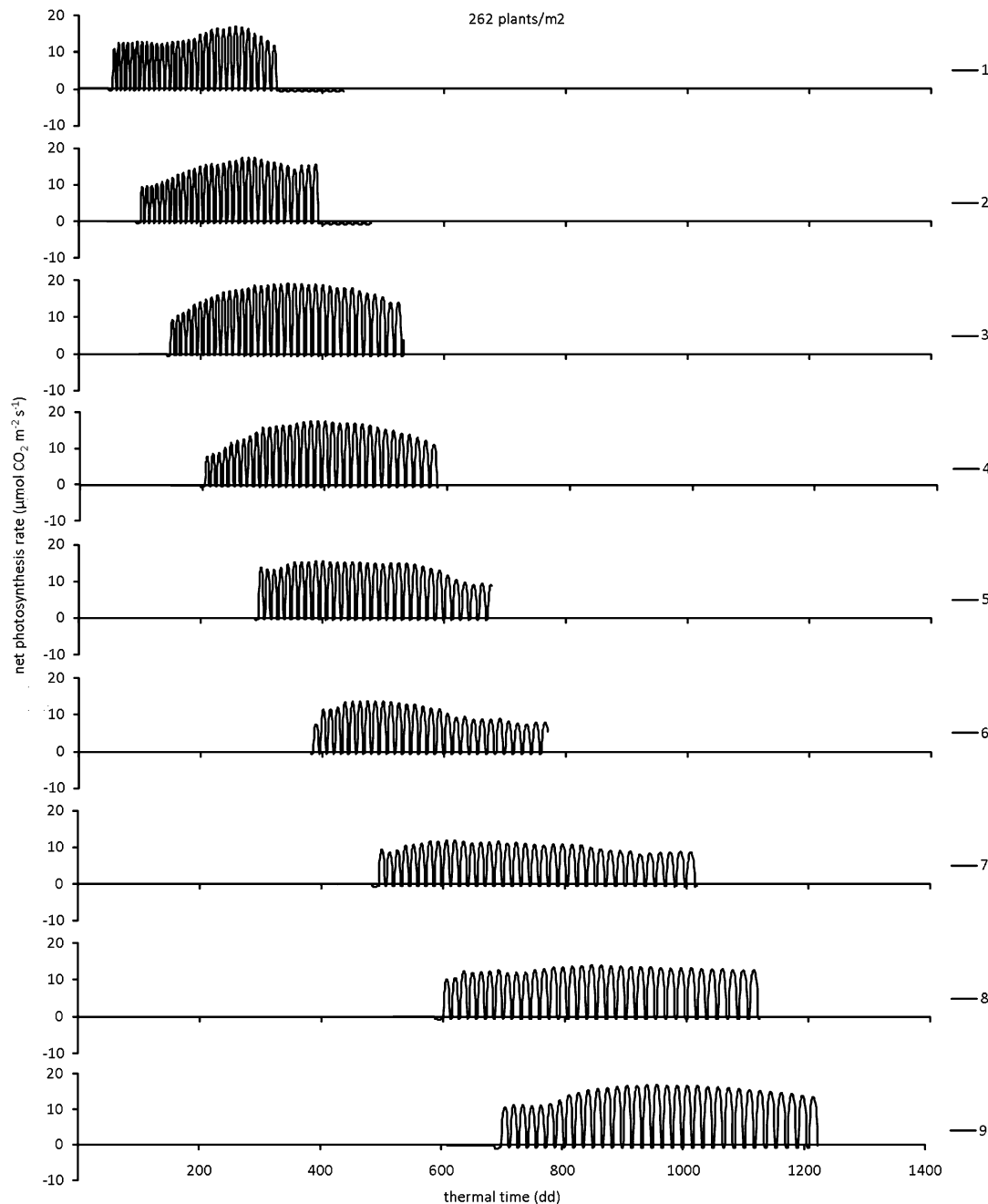


Fig. 3. Simulated net photosynthesis rate of individual leaves 1–9 on the main stem, versus thermal time from seedling emergence. Plant population density was 262 plants m^{-2} ; $n=16$.

higher using the realistic sky compared with the standard sky (9.7% and 11%, respectively). As a result final radiation use efficiency was lower: 1.45 $g MJ^{-1}$ using the realistic sky, compared with 1.84 $g MJ^{-1}$ for the standard sky.

Discussion

Evaluation of model performance

Simulated net photosynthesis rates of the individual leaves (Fig. 3) generally agreed with values found experimentally and are comparable with values found for wheat (Dreccer

et al., 2000; Yu *et al.*, 2002) and barley (Müller *et al.*, 2008). The somewhat abrupt end of leaf photosynthesis (Fig. 3) is due to the chosen implementation of leaf death (an empirical relationship with thermal time). The amount of allocated assimilates to individual organs was almost always lower than the demand for assimilates by the organs, as exemplified in Fig. 7. Only in the case of the topmost leaves did assimilate supply exceed organ demand. This was caused by the relatively large contribution of large well-lit leaves present in the canopy (top and penultimate leaves of most stems) leading to peaks in assimilation rate (Fig. 4) and ultimately an excess in acquired assimilates.

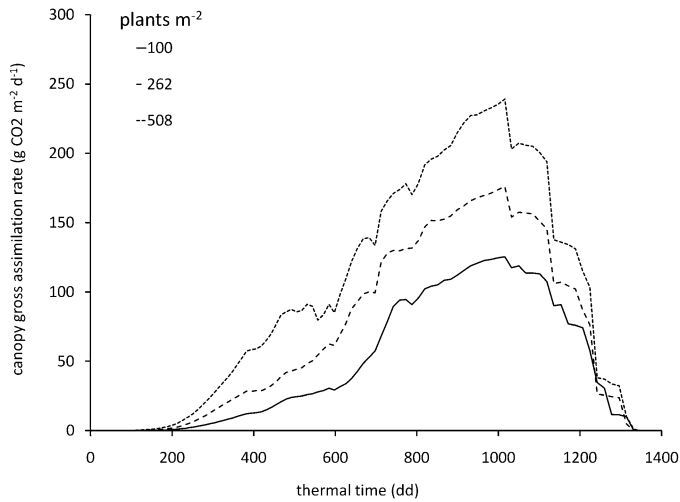


Fig. 4. Simulated canopy gross assimilation rate in grams of assimilated $\text{CO}_2 \text{ m}^{-2} \text{ ground area d}^{-1}$ versus thermal time, for three plant population densities (100, 262, and 508 plants m^{-2}); $n=16$.

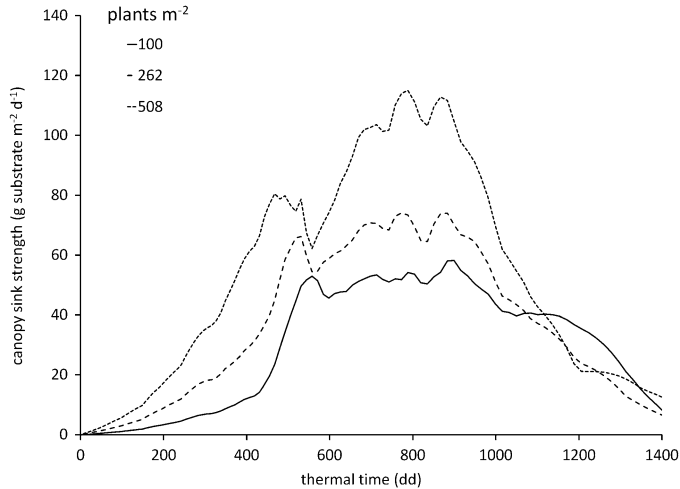


Fig. 5. Simulated canopy sink strength in grams of substrate $\text{m}^{-2} \text{ ground area d}^{-1}$ versus thermal time, for three plant population densities (100, 262, and 508 plants m^{-2}); $n=16$.

Crop-level output such as grain mass, above-ground biomass, and harvest index largely agree with values reported in the agronomic literature. Shearman *et al.* (2005) presented results on eight winter wheat cultivars grown at *c.* 200 plants m^{-2} , reporting values of 900–1100 g m^{-2} of grain mass, 1700–2000 g m^{-2} of above-ground mass, with resulting harvest indices ranging from 0.42 to 0.50. For winter wheat grown at the same plant population density of 200 plants m^{-2} , Darwinkel (1978) reported values of 830 g m^{-2} grain mass and 2024 g m^{-2} of above-ground mass (harvest index 0.41). Tripathi *et al.* (2004) reported average values of 860 g m^{-2} grain mass and 1730 g m^{-2} above-ground biomass (harvest index 0.44) for 16 genotypes grown at 200–300 plants m^{-2} . Values from the current study (in the case of 262 plants m^{-2} , which is closest to standard agricultural practice of the three plant population densities used) were 940 g m^{-2} of grain

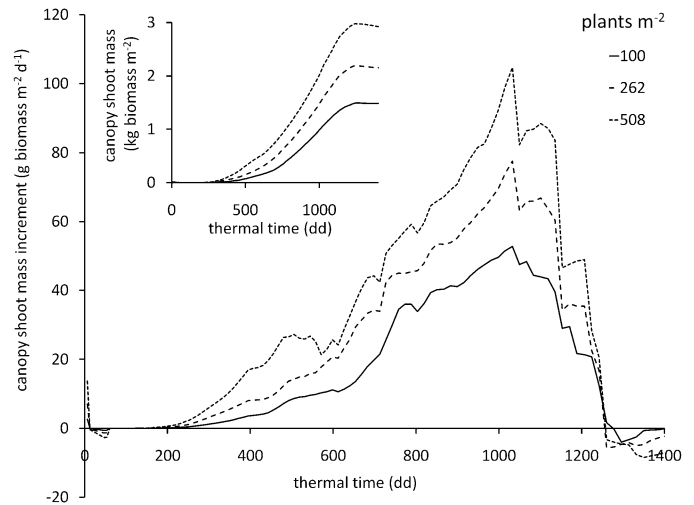


Fig. 6. Simulated canopy shoot mass increment in grams of biomass $\text{m}^{-2} \text{ d}^{-1}$ versus thermal time, for three plant population densities (100, 262, and 508 plants m^{-2}); $n=16$. The inset shows simulated canopy shoot mass in kg biomass m^{-2} .

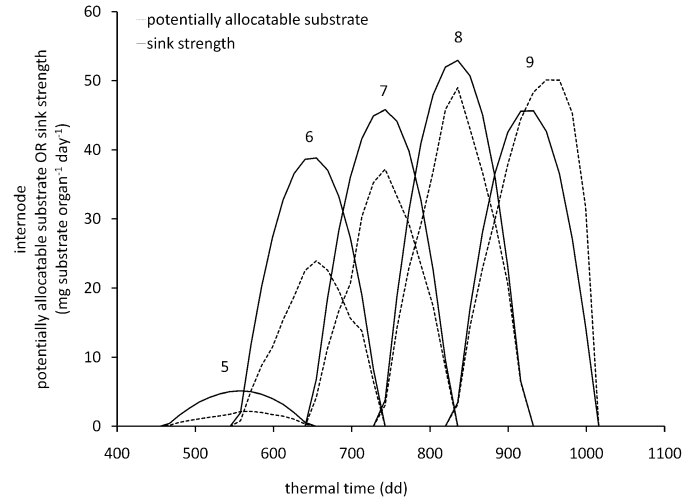


Fig. 7. Simulated potentially allocatable substrate and sink strength (both in $\text{mg substrate internode}^{-1} \text{ d}^{-1}$) for main stem internodes 5–9 versus thermal time. Plant population density was 262 plants m^{-2} ; $n=16$. The numbers above the peaks indicate the phytomer rank to which the data below it belongs.

mass, 2200 g m^{-2} of above-ground mass, and a resulting harvest index of 0.43. Therefore it is concluded that for this moderate plant population density, crop output variables were realistic. However, Darwinkel (1978) showed that population densities higher than 200 plants m^{-2} hardly increase grain mass and above-ground mass, due to lower grain numbers per ear at higher population densities. This effect of plant population density on grain number per ear was not taken into account in the current model implementation. The rather rigid sink strength function for ear growth used in this study therefore caused unrealistic crop-level output at high plant population densities. Improvements are needed on this aspect of plant development in relation to plant population density.

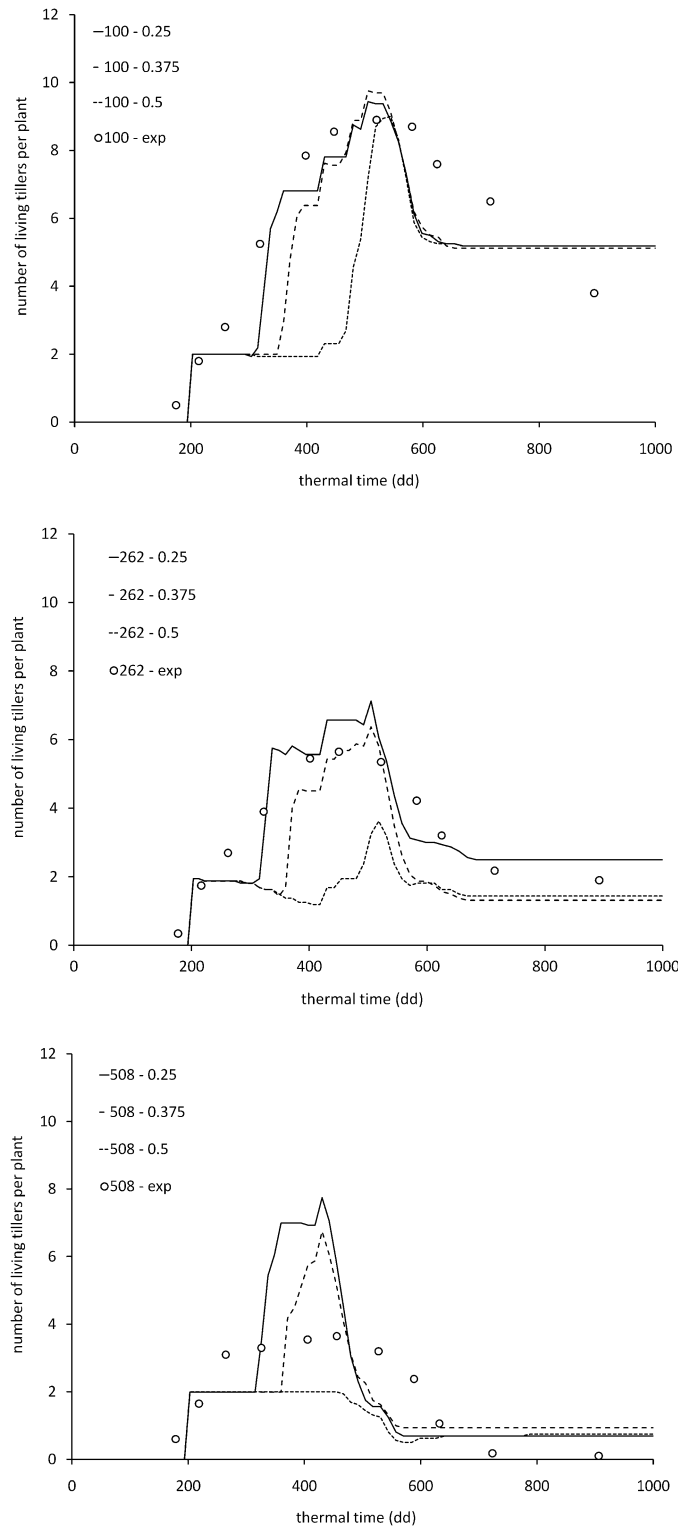


Fig. 8. (a, b, c) Number of living tillers per plant versus thermal time, for 100 (a), 262 (b), and 508 (c) plants m^{-2} ($n=16$) and three source/sink threshold values for tillering (0.25, 0.375, and 0.5); the open circles indicate experimental data ('exp') taken from Evers *et al.* (2006) ($n=20$).

Qualitatively, bud outgrowth dynamics were simulated well compared with the experimental values provided for the three different population densities, both in terms of tillers number per plant (Fig. 8) and moment of tiller

appearance (Fig. 9). Clearly, the output depended heavily on the value chosen for $j_{S/D}$ (the bud outgrowth threshold level of the source/sink ratio of the plants). The appropriate value for this parameter is difficult to determine experimentally. Dingkuhn *et al.* (2005) used an optimization method to find this threshold value in the case of rice (see also Luquet *et al.*, 2006). Their value of 1.0 or higher, depending on the rice cultivar and growing conditions, seem to be too high for wheat. A $j_{S/D}$ value of 1.0 or higher would mean that buds would only grow out when assimilate supply is equal to or in excess of assimilate demand. In wheat, tiller production appears to be much more opportunistic, even at conditions of high competition for resources, judging from the fact that wheat produces many tillers that do not survive to become grain-bearing shoots (Evers *et al.*, 2006). This phenomenon of tiller senescence seems to occur to a smaller extent in rice (Pasuquin *et al.*, 2008) than in wheat, suggesting contrasting strategies to optimize final tiller number between rice and wheat. However, simulation of the tiller life cycle (from bud outgrowth to tiller death) could be improved considerably by replacing the current empirical implementation of tiller senescence with mechanistic rules (e.g. Sparkes *et al.*, 2006), enabling tiller senescence to be simulated more realistically in diverse scenarios.

Bud outgrowth is not possible without resources. Hence, assimilate dependency of bud outgrowth, as implemented in the current study, is probably the most obvious putative mechanism: if supply of assimilates is sufficient, buds will develop into tillers, otherwise they do not. However, based on the literature, it is quite unlikely that assimilate dependency alone determines bud outgrowth in plants like wheat and other grasses and cereals. For example, experiments have shown that tiller production can be severely decreased by treating plants with additional far-red light (Casal, 1988; Skinner and Simmons, 1993). The existence of the light quality mediated shade-avoidance syndrome (Franklin, 2008) in itself is evidence that environmental signalling plays a decisive role in bud outgrowth. It seems sensible to suppose that environmental signals such as a low red to far-red ratio affect the way assimilates are distributed throughout the plants (Kasperbauer and Karlen, 1986) regulated by plant hormones (Leyser, 2009). Nevertheless, if shading does occur in spite of shade avoidance, a decrease in assimilation rate may cause further cessation of bud outgrowth. A next step in this research is to incorporate bud response to light quality through the way assimilates are distributed throughout the plants.

Modelling crop growth

One question arising from the work presented is whether FSPM is a suitable methodology to simulate and predict crop characteristics such as grain yield in wheat. A well-parameterized FSPM of wheat can be used for the same purposes as the more classical wheat crop growth models (e.g. Jamieson *et al.*, 1998; Van Ittersum *et al.*, 2003; Yin and Van Laar, 2005), in which leaf area, plant biomass, and

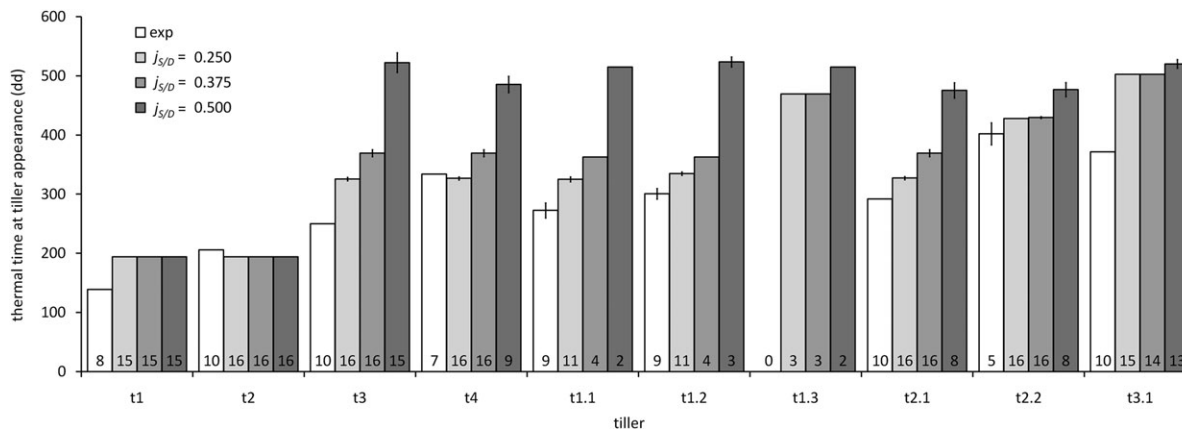


Fig. 9. Moment of tiller appearance, expressed as thermal time (dd) since plant emergence, for 262 plants m^{-2} and three source/sink threshold values for tillering (0.250, 0.375, and 0.500); the white bars ('exp') indicate data taken from the experiment described in this paper. The number at the bottom of each bar indicates the number of tillers that particular bar represents (i.e. sample size). Tiller codes: tx represents first order tillers originating from main stem phytomer x; tx.y represents second order tillers originating from phytomer y on tiller tx.

crop yield depend on resource capture (light, nutrients, water). However, if the modelling is motivated from such agronomic purposes, the classical models are more efficient tools to use than an FSPM because the parameter requirement of the latter is much larger than that of the former. FSPMs are therefore particularly suited to be used in cases where plant and canopy structure play an essential role in the research question. Examples of such cases are competition for resources between individual plants of the same or different species (for example, crop–weed competition in Cici *et al.*, 2008), manipulation of canopy structure such as plant cutting (Verdenal *et al.*, 2008) or pruning (Buck-Sorlin *et al.*, 2007), and the analysis of plant response to environmental conditions such as light (current study, and also Gautier *et al.*, 2000; Chelle *et al.*, 2007; Evers *et al.*, 2007a; Buck-Sorlin *et al.*, 2008). However, conclusions from such model studies are only relevant for a crop situation if the model can be shown to represent that reality sufficiently. We conclude that this is the case for our model.

Model sensitivity

Of the model input parameters tested, the sensitivity of final canopy biomass to changes in maximum organ biomass (W_{max}) and growth respiration (r_g) appeared to be only moderate (i.e. absolute elasticity was smaller than 1). The sign of the response (positive or negative) was in accordance with expectations: a higher W_{max} resulted in higher biomass production as growth was apparently not limited by the amount of light available for growth, within the range of W_{max} values tested. A higher r_g resulted in lower biomass production due to more substrates being used for growth respiration. The maximum number of tiller produced per plant appeared sensitive to modulation of W_{max} , τ , and r_g . Therefore, the value of these parameters needs to be chosen accurately if tiller production is the output variable of interest. Note that the sensitive response of tiller production

to the three parameters did not affect biomass production in a similarly sensitive way.

The negative elasticity of tiller number to modulation of W_{max} could be explained by the effect of W_{max} on the source/demand ratio (S/D) of the plants during growth: a higher W_{max} caused a higher total plant demand (equation 8), resulting in S/D values being more often below the threshold for tiller outgrowth, $j_{S/D}$, which subsequently leads to fewer tillers per plant. Similarly, a high r_g caused a higher total plant demand (equation 7), resulting in a negative effect on number of tillers produced. This simulation result implies the hypothesis that fewer tillers are produced in wheat cultivars with relatively large leaves compared to cultivars with small leaves. Perhaps the hypothesis can be extended to gramineous species with small leaves and many tillers (e.g. annual bluegrass: *Poa annua*) and those with large leaves and hardly any tillers (e.g. maize: *Zea mays*).

The current model appeared to be rather sensitive to the configuration of the light sources in the virtual hemisphere. The *c.* 40% higher light interception by the simulated crop using the more realistic sky compared with the standard sky was caused by the concentration of light intensity in the direct light (sun). The total amount of light in the simulation using the realistic sky was the same as using the standard sky, but more concentrated along the solar trajectory. This resulted in lower layers receiving more light compared to the standard sky situation; in addition most leaves were facing the solar track. The observation that this substantial difference in light interception did not lead to a similarly sized difference in biomass accumulation was caused by the fact that many leaves were light-saturated in the realistic-sky situation: there was no further increase in net photosynthesis rate with increasing light interception. It is a virtue of the type of FSPM reported in this paper that effects of 3D light regimes and 3D distributions of leaf area and photosynthetic properties in the canopy space can be assessed in detail.

Concluding remarks

This paper presented a detailed simulation model of spring wheat development integrating above-ground plant structure, organ-level microclimate, photosynthesis, assimilate distribution within the plant structure, and organ growth and development. More efforts are needed to model mechanistically other major physiological processes such as nitrogen uptake and distribution, and tiller and leaf senescence, which, in the present simulation, are merely present in the form of empirical relationships. Nevertheless, we consider the current work to be an important step forward towards an FSPM that integrates key aspects of plant form and function.

Supplementary data

The Supplementary data for this manuscript can be found at *JXB* online and contains a description of equations and their variables and parameters related to photosynthesis, stomatal conductance, organ microclimate, and global environment. They have been published previously (references are given in the main text) but are provided in order to have a complete documentation of the functional part of the wheat FSPM.

Acknowledgements

We thank A Schapendonk and S Pot of Plant Dynamics BV, T Pons and R Welschen of Utrecht University, and GWAM van der Heijden and G Polder of Biometris, Plant Research International, Wageningen UR for their technical support, the staff of the experimental facilities UNIFARM of Wageningen UR, F Sterk, and G Castel for their contributions to the experiments, and GH Buck-Sorlin, E Heuvelink, and PHB de Visser for scientific input. The Netherlands Organisation for Scientific Research (NWO) and the CT de Wit Graduate School for Production Ecology and Resource Conservation (PE&RC) provided financial support. The stay of P Romero at Wageningen University was partially financed by Instituto Nacional de Investigación y Tecnología Agraria y Alimentaria (INIA) with the project RTA2005-00103-00-00.

References

Bernacchi CJ, Portis AR, Nakano H, Von Caemmerer S, Long SP. 2002. Temperature response of mesophyll conductance. Implications for the determination of Rubisco enzyme kinetics and for limitations to photosynthesis *in vivo*. *Plant Physiology* **130**, 1992–1998.

Buck-Sorlin GH. 2002. L-system model of the vegetative growth of winter barley. In: Polani D, Kim J, Martinez T, eds. *Fifth German workshop on artificial life*. Lübeck, Germany: Akademische Verlagsgesellschaft Aka GmbH, Berlin, 53–64.

Buck-Sorlin G, Burema BS, Evers JB, van der Heijden GWAM, Heuvelink E, Marcelis LFM, Struik PC, de Visser PHB,

Damen THJ, Vos J. 2007. Virtual roses: a new tool to optimize plant architecture in glasshouse rose production systems. *5th international workshop on functional–structural plant models*. Napier, New Zealand, 48–1.

Buck-Sorlin G, Hemmerling R, Kniemeyer O, Burema B, Kurth W. 2008. A rule-based model of barley morphogenesis, with special respect to shading and gibberellic acid signal transduction. *Annals of Botany* **101**, 1109–1123.

Casal JJ. 1988. Light quality effects on the appearance of tillers of different order in wheat (*Triticum aestivum*). *Annals of Applied Biology* **112**, 167–173.

Chelle M, Andrieu B. 1998. The nested radiosity model for the distribution of light within plant canopies. *Ecological Modelling* **111**, 75–91.

Chelle M, Evers JB, Combes D, Varlet-Grancher C, Vos J, Andrieu B. 2007. Simulation of the three-dimensional distribution of the red:far-red ratio within crop canopies. *New Phytologist* **176**, 223–234.

Cici SZ-H, Adkins S, Hanan J. 2008. A canopy architectural model to study the competitive ability of chickpea with sowthistle. *Annals of Botany* **101**, 1311–1318.

Darwinkel A. 1978. Patterns of tillering and grain production of winter wheat at a wide range of plant densities. *Netherlands Journal of Agricultural Science* **26**, 383–398.

de Pury DGG, Farquhar GD. 1997. Simple scaling of photosynthesis from leaves to canopies without the errors of big-leaf models. *Plant, Cell and Environment* **20**, 537–557.

Dingkuhn M, Luquet D, De Reffye P, Quilot B. 2005. Environmental and genetic control of morphogenesis in crops: towards models simulating phenotypic plasticity. *Australian Journal of Agricultural Research* **56**, 1289–1302.

Dornbusch T, Wernecke P, Diepenbrock W. 2007. Description and visualization of graminaceous plants with an organ-based 3D architectural model, exemplified for spring barley (*Hordeum vulgare* L.). *The Visual Computer* **23**, 569–581.

Dreccer MF, Van Oijen M, Schapendonk AHCM, Pot CS, Rabbinge R. 2000. Dynamics of vertical leaf nitrogen distribution in a vegetative wheat canopy. Impact on canopy photosynthesis. *Annals of Botany* **86**, 821–831.

Drouet J-L, Pagès L. 2007. GRAAL-CN: A model of GRowth, Architecture and ALlocation for Carbon and Nitrogen dynamics within whole plants formalised at the organ level. *Ecological Modelling* **206**, 231–249.

Evers JB, Vos J, Andrieu B, Struik PC. 2006. Cessation of tillering in spring wheat in relation to light interception and red:far-red ratio. *Annals of Botany* **97**, 649–658.

Evers JB, Vos J, Chelle M, Andrieu B, Fournier C, Struik PC. 2007 a. Simulating the effects of localized red:far-red ratio on tillering in spring wheat (*Triticum aestivum*) using a three-dimensional virtual plant model. *New Phytologist* **176**, 325–336.

Evers JB, Vos J, Fournier C, Andrieu B, Chelle M, Struik PC. 2005. Towards a generic architectural model of tillering in Gramineae, as exemplified by spring wheat (*Triticum aestivum*). *New Phytologist* **166**, 801–812.

- Evers JB, Vos J, Fournier C, Andrieu B, Chelle M, Struik PC.** 2007. *b.* An architectural model of spring wheat: evaluation of the effects of population density and shading on model parameterization and performance. *Ecological Modelling* **200**, 308–320.
- Farquhar GD, von Caemmerer S, Berry JA.** 1980. A biochemical model of photosynthetic CO₂ assimilation in leaves of C₃ species. *Planta* **149**, 78–90.
- Fourcaud T, Zhang X, Stokes A, Lambers H, Korner C.** 2008. Plant growth modelling and applications: the increasing importance of plant architecture in growth models. *Annals of Botany* **101**, 1053–1063.
- Fournier C, Andrieu B.** 1999. ADEL-maize: an L-system based model for the integration of growth processes from the organ to the canopy. Application to regulation of morphogenesis by light availability. *Agronomie* **19**, 313–327.
- Fournier C, Andrieu B, Buck-Sorlin G, Evers JB, Drouet J-L, Escobar-Gutiérrez A, Vos J.** 2007. Functional–structural modelling of Gramineae. In: Vos J, Marcelis LFM, de Visser PHB, Struik PC, Evers JB, eds. *Functional–structural plant modelling in crop production*, Vol. 22. Dordrecht, the Netherlands: Springer, 175–186.
- Fournier C, Andrieu B, Ljutovac S, Saint-Jean S.** 2003. ADEL-wheat: a 3D architectural model of wheat development. In: Hu BG, Jaeger M, eds. *2003' International symposium on plant growth modelling, simulation, visualization, and their applications*. Beijing, China PR: Tsinghua University Press/Springer, 54–63.
- Franklin KA.** 2008. Shade avoidance. *New Phytologist* **179**, 930–944.
- Gautier H, Měch R, Prusinkiewicz P, Varlet-Grancher C.** 2000. 3D Architectural modelling of aerial photomorphogenesis in white clover (*Trifolium repens* L.) using L-systems. *Annals of Botany* **85**, 359–370.
- Godin C, Sinoquet H.** 2005. Functional-structural plant modelling. *New Phytologist* **166**, 705–708.
- Goudriaan J, Van Laar HH.** 1994. *Modelling potential crop growth processes*. Dordrecht: Kluwer Academic Publishers.
- Guo Y, Ma Y, Zhan Z, Li B, Dingkuhn M, Luquet D, De Reffye P.** 2006. Parameter optimization and field validation of the functional-structural model GREENLAB for maize. *Annals of Botany* **97**, 217–230.
- Heuvelink E.** 1996. Dry matter partitioning in tomato: validation of a dynamic simulation model. *Annals of Botany* **77**, 71–80.
- Jamieson PD, Porter JR, Goudriaan J, Ritchie JT, van Keulen H, Stol W.** 1998. A comparison of the models AFRCWHEAT2, CERES-Wheat, Sirius, SUCROS2 and SWHEAT with measurements from wheat grown under drought. *Field Crops Research* **55**, 23–44.
- Kasperbauer MJ, Karlen DL.** 1986. Light-mediated bioregulation of tillering and photosynthate partitioning in wheat. *Physiologia Plantarum* **66**, 159–163.
- Leyser O.** 2009. The control of shoot branching: an example of plant information processing. *Plant, Cell and Environment* **32**, 694–703.
- Luquet D, Dingkuhn M, Kim H, Tambour L, Clement-Vidal A.** 2006. EcoMeristem, a model of morphogenesis and competition among sinks in rice. 1. Concept, validation and sensitivity analysis. *Functional Plant Biology* **33**, 309–323.
- Matthews RB, Hunt LA.** 1994. GUMCAS: A model describing the growth of cassava (*Manihot esculenta* L. Crantz). *Field Crops Research* **36**, 69–84.
- Měch R.** 2004. *CPFG Version 4.0 User's Manual*. Calgary, Canada: University of Calgary, 129.
- Monteith JL.** 1973. *Principles of environmental physics*. London: Edward Arnold, 241.
- Müller J, Braune H, Diepenbrock W.** 2008. Photosynthesis-stomatal conductance model LEAFC3-N: specification for barley, generalised nitrogen relations, and aspects of model application. *Functional Plant Biology* **35**, 797–810.
- Pasuquin E, Lafarge T, Tubana B.** 2008. Transplanting young seedlings in irrigated rice fields: Early and high tiller production enhanced grain yield. *Field Crops Research* **105**, 141–155.
- Penning de Vries FWT, Jansen DM, ten Berge HFM, Bakema A.** 1989. *Simulation of ecophysiological processes of growth in several annual crops*. Wageningen, the Netherlands: Pudoc.
- Prusinkiewicz P, Karwowski R, Měch R, Hanan JS.** 2000. L-studio/CPFG: a software system for modelling plants. In: Nagl M, Schürr A, Münch M, eds. *Applications of graph transformations with industrial relevance. Lecture notes in computer science 1779*. Berlin, Germany: Springer, 457–464.
- Room PM, Hanan JS, Prusinkiewicz P.** 1996. Virtual plants: new perspectives for ecologists, pathologists and agricultural scientists. *Trends in Plant Science* **1**, 33–38.
- Shearman VJ, Sylvester-Bradley R, Scott RK, Foulkes MJ.** 2005. Physiological processes associated with wheat yield progress in the UK. *Crop Science* **45**, 175–185.
- Skinner RH, Simmons SR.** 1993. Modulation of leaf elongation, tiller appearance and tiller senescence in spring barley by far-red light. *Plant, Cell and Environment* **16**, 555–562.
- Sparkes DL, Holme SJ, Gaju O.** 2006. Does light quality initiate tiller death in wheat? *European Journal of Agronomy* **24**, 212–217.
- Tripathi SC, Sayre KD, Kaul JN, Narang RS.** 2004. Lodging behavior and yield potential of spring wheat (*Triticum aestivum* L.): effects of ethephon and genotypes. *Field Crops Research* **87**, 207–220.
- Van Ittersum MK, Leffelaar PA, Van Keulen H, Kropff MJ, Bastiaans L, Goudriaan J.** 2003. On approaches and applications of the Wageningen crop models. *European Journal of Agronomy* **18**, 201–234.
- Verdenal A, Combes D, Escobar-Gutiérrez AJ.** 2008. A study of ryegrass architecture as a self-regulated system, using functional–structural plant modelling. *Functional Plant Biology* **35**, 911–924.
- Vos J.** 1981. *Effects of temperature and nitrogen supply on post-floral growth of wheat; measurements and simulations*. Wageningen: PUDOC.
- Vos J, Evers JB, Buck-Sorlin GH, Andrieu B, Chelle M, de Visser PHB.** 2009. Functional–structural plant modelling: a new versatile tool in crop science. *Journal of Experimental Botany* doi: 10.1093/jxb/erp1345.
- Watanabe T, Hanan JS, Room PM, Hasegawa T, Nakagawa H, Takahashi W.** 2005. Rice morphogenesis and plant architecture: measurement, specification and the reconstruction of structural

development by 3D architectural modelling. *Annals of Botany* **95**, 1131–1143.

Williams RF, Langer RHM. 1975. Growth and development of the wheat tiller bud. II. The dynamics of tiller growth. *Australian Journal of Botany* **23**, 745–759.

Yin X, Goudriaan J, Lantinga EA, Vos J, Spiertz HJ. 2003. A flexible sigmoid function of determinate growth. *Annals of Botany* **91**, 361–371.

Yin X, Struik PC. 2009. C3 and C4 photosynthesis models: an overview from the perspective of crop modelling. *NJAS Wageningen Journal of Life Sciences* doi: 10.1016/j.njas.2009.1007.1001.

Yin X, Struik PC, Romero P, Harbinson J, Evers JB, van der Putten PEL, Vos J. 2009. Using combined measurements of gas exchange and chlorophyll fluorescence to estimate parameters of

a biochemical C₃ photosynthesis model: a critical appraisal and a new integrated approach applied to leaves in a wheat (*Triticum aestivum*) canopy. *Plant, Cell and Environment* **32**, 448–464.

Yin X, Van Laar HH. 2005. *Crop systems dynamics: an ecophysiological simulation model for genotype-by-environment interactions*. Wageningen: Wageningen Academic Publishers.

Yin X, Van Oijen M, Schapendonk AHCM. 2004. Extension of a biochemical model for the generalized stoichiometry of electron transport limited C₃ photosynthesis. *Plant, Cell and Environment* **27**, 1211–1222.

Yu Q, Liu Y, Liu J, Wang T. 2002. Simulation of leaf photosynthesis of winter wheat on Tibetan Plateau and in North China Plain. *Ecological Modelling* **155**, 205–216.